arXiv:2511.17185v2 [cs.CV] 29 May 2026

PostCam: Camera-Controllable Novel-View Video Generation with Query-Shared Cross-Attention

Yipeng Chen*
State Key Lab of CAD&CG, Zhejiang University
China

Zhichao Ye*
Shanghai InSpatio Intelligent Technology Co., Ltd.
China

Zhenzhou Fan
State Key Lab of CAD&CG, Zhejiang University
China

Xinyu Chen
State Key Lab of CAD&CG, Zhejiang University
China

Xiaoyu Zhang
Shanghai InSpatio Intelligent Technology Co., Ltd.
China

Jialing Liu
Shanghai InSpatio Intelligent Technology Co., Ltd.
China

Nan Wang
Shanghai InSpatio Intelligent Technology Co., Ltd.
China

Guofeng Zhang†
State Key Lab of CAD&CG, Zhejiang University
China

Haomin Liu
Shanghai InSpatio Intelligent Technology Co., Ltd.
China

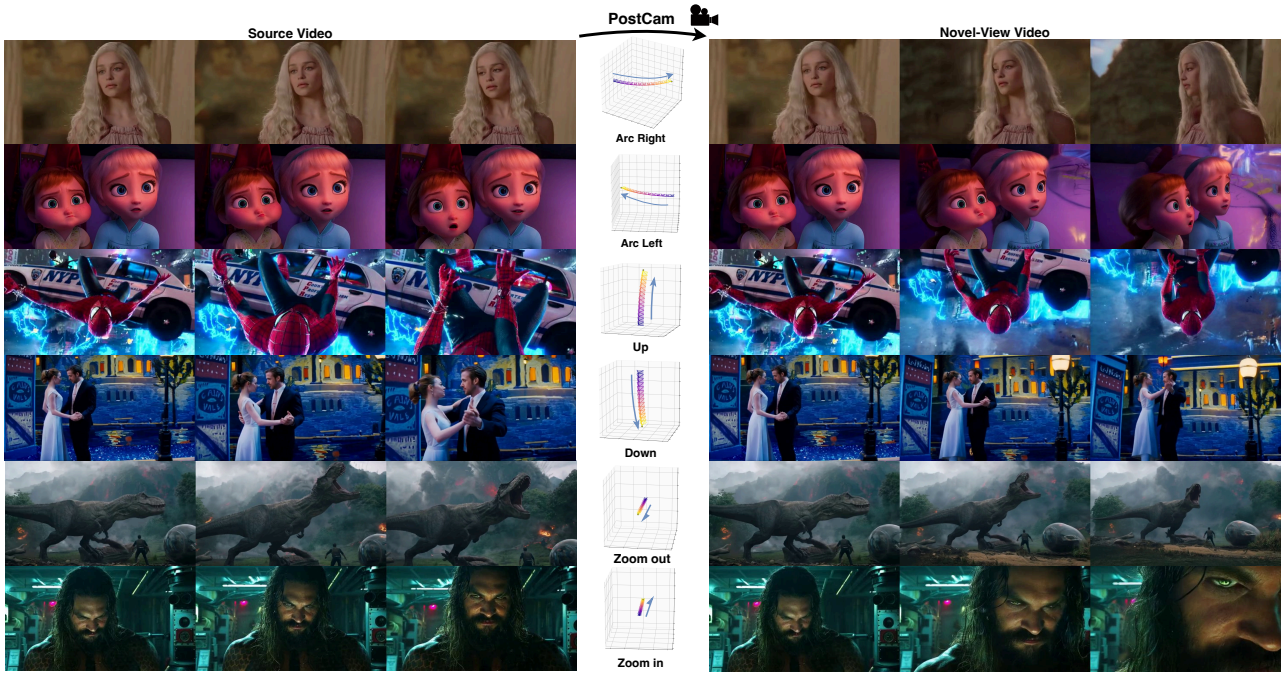


Figure 1: Given a source video (left) and a target camera trajectory (middle), PostCam generates high-quality novel-view videos (right), enabling post-capture editing of camera motion in dynamic scenes. Despite employing a lightweight backbone with only 1.3B parameters, PostCam achieves precise trajectory control and high-fidelity novel-view synthesis across a wide range of video styles and motion patterns.

*Equal Contribution.
†Corresponding Authors.

Permission to make digital or hard copies of all or part of this work for personal or classroom use is granted without fee provided that copies are not made or distributed for profit or commercial advantage and that copies bear this notice and the full citation on the first page. Copyrights for components of this work owned by others than the author(s) must be honored. Abstracting with credit is permitted. To copy otherwise, or republish, to post on servers or to redistribute to lists, requires prior specific permission and/or a fee. Request permissions from permissions@acm.org.
ACM MM '26, Rio de Janeiro, Brazil
© 2026 Copyright held by the owner/author(s). Publication rights licensed to ACM.
ACM ISBN 978-1-4503-XXXX-X/2026/11
https://doi.org/XXXXXXX.XXXXXXX

Abstract

We propose PostCam, a streamlined framework for novel-view video generation that achieves superior detail preservation and precise camera trajectory editing in dynamic scenes. Current methods often struggle with a trade-off between pose-based control, which lacks visual detail, and rendering-based guidance, which is overly sensitive to geometric accuracy. Despite recent hybrid attempts, achieving precise motion and visual consistency remains challenging due to the lack of effective cross-modal alignment. We argue that robust control stems from the deep alignment of multimodal signals rather than increased input complexity. Our core contribution is the Query-Shared Cross-Attention mechanism, which projects 6-DoF poses and rendered features into a unified latent space. This allows the model to spontaneously achieve intrinsic consistency between motion cues and pixel-level guidance during denoising. Experiments demonstrate that PostCam maintains high-fidelity visual details while outperforming state-of-the-art methods by 20% in trajectory precision, exhibiting superior robustness in complex dynamic scenes.

Keywords

novel-view video generation, camera control, video diffusion model, cross-attention

ACM Reference Format:

Yipeng Chen, Zhichao Ye, Zhenzhou Fan, Xinyu Chen, Xiaoyu Zhang, Jialing Liu, Nan Wang, Guofeng Zhang, and Haomin Liu. 2026. PostCam: Camera-Controllable Novel-View Video Generation with Query-Shared Cross-Attention. In *Proceedings of Proceedings of the 34th ACM International Conference on Multimedia (ACM MM '26).* ACM, Rio de Janeiro, Brazil, 13 pages. https://doi.org/XXXXXXX.XXXXXXX



Figure 2: Comparison with State-of-the-Art Methods in Real Dynamic Scenes. We compare the last-frame results of state-of-the-art methods with those of our approach, using the last frame of the source video (first column) as a reference. Across all examples, our method consistently preserves fine details (e.g., faces, hands), whereas existing methods often suffer from blurring, distortion, and identity drift. Moreover, our approach remains robust even in challenging cases where other methods fail completely (rows 4–5), producing high-quality and temporally coherent results. For additional comparisons, please refer to our supplementary videos.

1 Introduction

Recent years have witnessed remarkable progress in video generation models [6, 28, 35, 43, 49], with substantial improvements in both fidelity and diversity. Consequently, research has increasingly focused on controllable video generation to meet the demands of professional production. Among various control signals, camera motion is fundamental as it defines the viewpoint trajectory and narrative rhythm. However, high-end camera effects typically require expensive hardware, making "post-capture editing" of camera trajectories a highly sought-after, yet challenging task that demands strict temporal synchronization and spatial consistency.

Current research in camera-controllable generation often oscillates between two technical paradigms, each with inherent limitations. Pose-based methods [3] encode trajectories in numerical embeddings, which provides flexible control but often fails to preserve intricate visual details, leading to identity drift or blurriness. In contrast, rendering-based approaches [25] lift source videos into 3D proxy representations for visual guidance; however, these methods are overly sensitive to the accuracy of geometric priors (e.g., depth estimation), where minor errors can trigger severe artifacts. Although recent hybrid attempts [7, 8] combine both signals via latent concatenation, they still suffer from significant motion deviations and detail inconsistencies due to the lack of an effective cross-modal alignment mechanism.

We argue that the key to achieving robust and precise control lies not in increasing the complexity of auxiliary inputs, but in the deep alignment of multimodal control signals. To this end, we propose PostCam, a streamlined and efficient framework for novel-view video generation. The core innovation is the Query-Shared Cross-Attention (QSCA) mechanism. By projecting 6-DoF poses and rendered features into a unified latent space, QSCA enables the model to spontaneously achieve intrinsic consistency between motion cues and pixel-level guidance during the denoising process. To facilitate better convergence, we further adopt a two-stage training strategy that decouples coarse motion learning from fine-grained appearance refinement.

Experimental results demonstrate that PostCam achieves superior detail preservation while outperforming state-of-the-art methods by over 20% in trajectory precision. Our framework exhibits remarkable robustness in complex dynamic scenes, providing a high-fidelity solution for post-capture camera editing.

In summary, our contributions are summarized as follows:

- We propose **PostCam**, a streamlined framework for novel-view video generation that enables precise camera trajectory editing while maintaining high-fidelity visual details in dynamic scenes.
- We introduce the **Query-Shared Cross-Attention (QSCA)** mechanism, which achieves deep alignment between 6-DoF

poses and rendered features within a unified latent space, ensuring intrinsic consistency in motion control.
- We propose a **two-stage training strategy** that effectively decouples motion acquisition and appearance refinement, significantly enhancing generation quality.
- Extensive experiments show that PostCam outperforms state-of-the-art methods by 20% in camera-control accuracy and view consistency, achieving superior performance on both real and synthetic datasets.

2 Related Work

2.1 Video Generation.

Our method builds upon video diffusion models, which have emerged as the prevailing paradigm for video generation. VDM [15] pioneered the application of diffusion models to high-resolution video synthesis. In recent years, video diffusion architectures have transitioned from U-Net designs [5, 11, 32] to transformer-based architectures [6, 19, 35, 43, 49], enabling greater realism and dynamic fidelity. Among them, Wan2.1 [35] demonstrates superior generation capability as an open-source model and is therefore selected as our backbone.

2.2 Camera-Controllable Video Generation.

Camera-controllable video generation was initially advanced within the frameworks of text-to-video and image-to-video synthesis. As a pioneering work, MotionCtrl [39] encodes 6-DoF camera poses and injects them into the diffusion model, fine-tuning on paired video-camera data to achieve video generation with arbitrary trajectory control. Several subsequent works [1, 2, 12, 20, 22, 37, 42, 48] enhance camera accuracy by introducing Plücker embeddings to represent camera configurations. Nevertheless, learning camera-motion control solely from numerical or Plücker representations is challenging, as it requires cross-modal interaction between visual information and numerical signals. Beyond direct camera-pose conditioning, many approaches [9, 10, 21, 26, 29, 30, 45, 46] instead leverage point-cloud-rendered videos for camera-motion control: monocular depth is first lifted to a 3D point cloud, after which a proxy video is rendered from the target camera pose and injected into the network as a strong visual constraint. DaS [10] takes this further by replacing the RGB render with a 3D point-trajectory video, endowing the diffusion model with intrinsic 3D awareness. Some image-to-video methods, such as MVGenMaster [7] and Uni3C [8], attempt simple modal fusion by combining Plücker coordinates (from camera poses) with rendered videos in the latent space via addition and channel concatenation. Furthermore, several training-free methods have been proposed [16, 17, 23, 41]. Overall, these methods achieve a degree of camera control, yet they remain restricted to reference-image or prompt-based generation and cannot synthesize results conditioned on a given source video.

2.3 Novel-View Video Generation.

Novel-view video generation with camera control has been pursued along two main avenues. Pose-based methods condition a diffusion model on extrinsic camera parameters. GCD [34] pioneers camera-controllable video-to-video generation by training on synthetically paired data from the Kubric simulator; however, its performance degrades under the large domain gap between synthetic and real videos. ReCamMaster [3] augments the noised latent with encoded pose vectors, yet the implicit injection inevitably perturbs visual quality. A common limitation of these approaches is the weak cross-modal alignment between purely numerical pose signals and rich visual content, resulting in imprecise trajectories and limited fidelity. Rendering-based methods [4, 25, 40, 44, 47] circumvent direct parameter injection by constructing an explicit 3D proxy. TrajectoryCrafter [25] lifts the source video into a point cloud via monocular depth estimation, renders a proxy video from the target camera, and uses this rendered video as a strong visual condition. Although impressive control is achieved when the depth map is accurate, depth errors propagate into texture drift or ghosting artifacts that corrupt the final output. These rendering-based methods [4, 25, 40, 44, 47] share the same fragility: imperfect or incomplete point clouds severely degrade video quality. In contrast to our task (which involves re-generating a video from a new viewpoint based on an input video), CameraCtrl II [13] is dedicated to dynamic scene exploration, which it achieves by iteratively generating the next coherent video clip conditioned on the previous one. In summary, pose-based techniques suffer from weak visual–pose alignment, whereas rendering-based techniques are critically sensitive to depth accuracy. Both paradigms currently fail to simultaneously deliver robust pose control and high-fidelity results in real-world scenes.

3 Method

3.1 Preliminary: Base Model.

We adopt Wan2.1 [35] as the backbone, a flow matching [24] framework built upon the prevailing diffusion transformer. It comprises three key components: Wan-VAE, a diffusion transformer, and a text encoder.

Given an input video x_0, the Wan-VAE compresses it into the latent space z_0. The model learns the conditional distribution $p(z_0|c_{\text{txt}})$, where c_{txt} denotes the text prompt. Wan2.1 employs flow matching to define the forward process with straight paths from the data distribution to the standard normal distribution:

$$z_t = (1-t)z_0 + t\epsilon, \quad \epsilon \sim \mathcal{N}(0, I) \tag{1}$$

where t represents the diffusion timestep and the noised latent z_t is constructed by adding random noise to z_0. The model predicts the velocity field $\mathcal{V}_\theta$ through:

$$\min_\theta \mathbb{E}_{z_0,t,\epsilon,c_{\text{txt}}} \left[\|\mathcal{V}_\theta(z_t, t, c_{\text{txt}}) - (\epsilon - z_0)\|^2 \right] \tag{2}$$

3.2 Overview.

The objective is to learn a model that generates a novel-view target video x_{tgt}, conditioned on a source video x_{src} and a target camera trajectory c_{cam}. Specifically, we model the conditional distribution $p(z_0 \mid c_{\text{txt}}, c_{\text{cam}}, z_{\text{src}})$, where $z_0 \in \mathbb{R}^{c\times(f\times h\times w)}$ is the latent representation of the target video, $z_{\text{src}} \in \mathbb{R}^{c\times(f\times h\times w)}$ is the latent of the source video, c_{txt} denotes the text condition, and c_{cam} represents the camera condition. The symbols c, f, h, and w denote the channel count, temporal frames, spatial height, and width of the latent features after VAE encoding and patch tokenization.

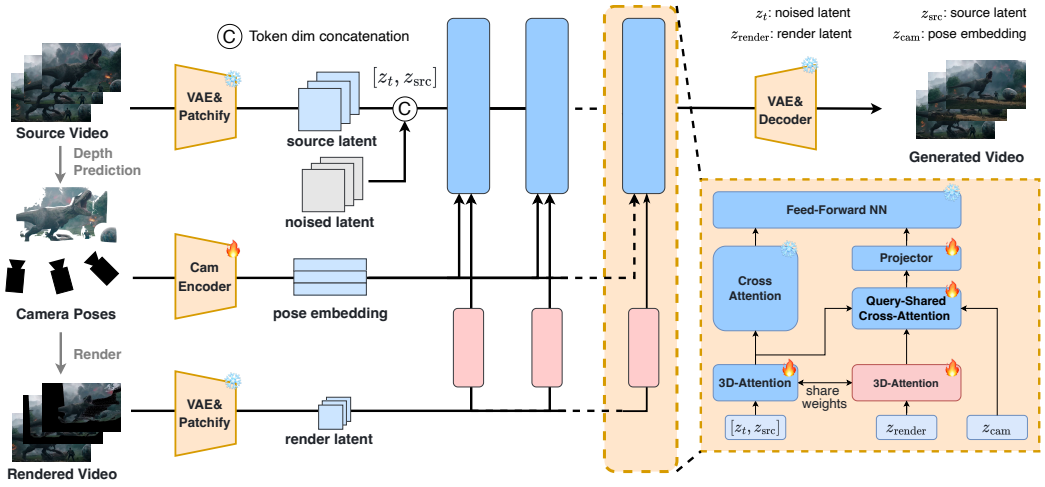


Figure 3: Framework overview. The model stacks multiple transformer blocks along three parallel pathways. (a) The source video is first encoded into latent space and then concatenated with the noised latents before entering the transformer blocks. (b) The camera parameters are processed by a lightweight encoder and injected into every block via query-shared cross-attention. The specific implementation details of this query-shared cross-attention mechanism are further elaborated in Fig. 4. (c) The rendered video is similarly encoded into latent space; within each block, it undergoes self-attention to extract high-level visual features. An exploded view (bottom right) depicts the internal structure of a transformer block.

As shown in Fig. 3, the text-to-video backbone is extended with three additional inputs: the source video, the camera trajectory, and a rendered video. The source video, serving as a visual reference for both appearance and motion dynamics, is first encoded by a variational autoencoder and tokenized into patches. The resulting latent representation is concatenated with the noised latent along the token dimension to form $[z_t, z_{\text{src}}] \in \mathbb{R}^{c\times(2f\times h\times w)}$, and the concatenated latent is processed by a self-attention mechanism to extract high-level visual representations. The camera conditions consist of two modalities: the rendered video and the camera trajectory. The proposed query-shared cross-attention jointly injects both modalities into the noised latent, effectively incorporating camera motion information during denoising.

The training objective is given by:

$$\min_{\theta} \mathbb{E}_{z_0,t,\epsilon,c_{\text{txt}},c_{\text{cam}},z_{\text{src}}} \Big[\|\mathcal{V}_\theta(z_t,\ t,\ c_{\text{txt}},\ c_{\text{cam}},\ z_{\text{src}}) - (\epsilon - z_0)\|^2 \Big] \tag{3}$$

3.3 Camera Condition Preprocessing.

Before injecting the camera conditions into the noised latents, we perform distinct preprocessing for the camera parameters and the rendered video.

For the camera poses, a lightweight camera encoder is trained to map the camera extrinsic matrix $\mathbf{c}_{\text{cam}}$ to a pose embedding $\mathbf{z}_{\text{cam}} \in \mathbb{R}^{c\times f}$. To preserve temporal consistency, 1D Rotary Positional Embeddings (RoPE) are applied during the subsequent cross-attention stage.

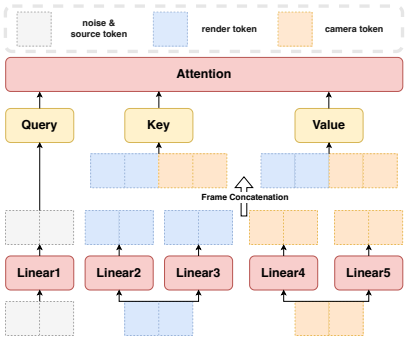


Figure 4: Query-shared cross-attention mechanism.

The rendered video is generated by first lifting the source video into 3D via monocular depth estimation and then reprojecting it along the target camera trajectory. While existing methods rely on full-resolution rendering, we observe that within our query-shared mechanism, the primary role of the rendered video is to refine motion accuracy and enhance visual fidelity, rather than to achieve precise pixel-wise correspondence. This also explains why the model can still produce correct motion even when inaccurate depth maps lead to severely distorted rendering. Therefore, we downsample the rendered video in the spatial dimensions, reducing computational cost without compromising the quality of the generated output. The downsampled rendered video is encoded together with the source video by the same VAE, after which high-level visual features are extracted through 3D self-attention, yielding $z_{\text{render}} \in \mathbb{R}^{c\times(f\times\frac{h}{4}\times\frac{w}{4})}$. This self-attention module reuses the weights of the backbone without introducing additional parameters.

3.4 Query-Shared Cross-Attention

To suppress extraneous cues from the dual-modality camera condition, we propose a novel query-shared cross-attention module. Within each transformer block, the camera condition is injected into the noised latent via the proposed cross-attention mechanism.

In query-shared cross-attention, the query vector is obtained by applying a linear projection to z_t:

$$Q = \text{Linear}(z_t).$$

Simultaneously, z_{render} and z_{cam} are each linearly projected to produce the corresponding keys (K_{render} and K_{cam}) and values (V_{render} and V_{cam}).

The keys and values from both conditions are concatenated along the token dimension, and attention is computed as:

$$A = \text{softmax}\left(\frac{Q\,[K_{\text{render}},\ K_{\text{cam}}]^{\top}_{\text{token-dim}}}{\sqrt{d_q}}\right) \tag{4}$$

where d_q is the dimensionality of the query. The module first computes an attention matrix from the query and the concatenated key features. A subsequent softmax operation produces a weighted distribution, assigning higher importance to features most relevant to the video generation task. These weights govern the selective aggregation of information from the concatenated value features, allowing the module to distill common camera motion cues for both precise pose control and high-fidelity generation. The resulting attention output is projected and added back to the noised latent:

$$z_t = z_t + \text{projector}\Big(A\,[V_{\text{render}},\ V_{\text{cam}}]_{\text{token-dim}}\Big) \tag{5}$$

3.5 Training Strategy

To preserve the video-generation capability of the base model, almost all parameters are frozen. Only the self-attention modules are updated to integrate information from the source latent into the noised latent, ensuring spatiotemporal consistency between them. Additionally, we introduce three trainable modules beyond the base architecture: a camera encoder, a query-shared cross-attention block, and a lightweight projector.

In practice, we adopt a two-stage training strategy that enables the model to learn low-frequency camera-motion cues while avoiding interference from rendered visual signals during the early training phase: *Stage 1: Pose-Only Conditioning Phase.* In this phase, only the camera extrinsic parameters are used; no rendered video is provided. The camera features are injected as:

$$z_t = z_t + \text{projector}\left(\text{softmax}\left(\frac{QK_{\text{cam}}^{T}}{\sqrt{d_q}}\right)V_{\text{cam}}\right) \tag{6}$$

The projection layer is initialized to zero, effectively suppressing the influence of the camera-control signal during early training. This allows the model to first learn content injection from the source video before acquiring camera-motion control capability. Without the projector module, the model struggles to converge, as it must learn both source injection and camera motion extraction from the extrinsic parameters simultaneously. *Stage 2: Joint Conditioning Phase.* In this phase, after the model has acquired coarse camera-control ability, both camera poses and rendered video are provided during training. The model now benefits from the complementary nature of the two conditions, leading to improved control precision and overall generation quality.

4 Experimental Results

4.1 Experimental Setup.

Training Details. For a fair comparison, the model is trained on the same synthetic dataset as ReCamMaster [3], with a learning rate of 1×10^{-5}. The training is conducted on 8 NVIDIA H200 GPUs with a batch size of 2 per GPU, resulting in a total batch size of 16. The training process consists of two phases: in the first phase, the model is trained exclusively with camera poses until loss convergence; in the second phase, it undergoes joint training with both camera poses and rendered videos until reaching a final converged state. The additional parameters introduced include a linear projector and a cross-attention module within each DiT block, alongside a lightweight camera encoder composed of four linear layers. Following the experimental setup of ReCamMaster, we employ Wan2.1-1.3B [35] as our base model. Since most state-of-the-art video generation backbones share similar DiT-style architectures, our method is inherently generalizable to other foundational frameworks.

Evaluation Dataset. To enable accurate and comprehensive evaluation, we construct both real and synthetic test sets. The real-world set includes 100 clips from OpenViD [27], each paired with 10 basic camera trajectories following the testing protocol of ReCamMaster, resulting in 1,000 test samples. Since ground-truth videos are unavailable in real-world scenes, we additionally generate a synthetic test set following the pipeline of ReCamMaster, enabling direct comparison between generated and ground-truth videos. Consisting of 100 samples across ten dynamic scenes, the synthetic dataset features intricate composite trajectories, in contrast to the ten basic camera movements. Examples and further details can be found in the supplementary material.

Evaluation Metrics. *(1) Camera Accuracy:* To evaluate the camera motion control accuracy of different models, we estimate the camera trajectory of the generated video and compare it with the ground-truth trajectory, computing the rotation error (RotErr) and translation error (TransErr). Since conventional pose estimation methods (e.g., COLMAP and GLOMAP) often fail in dynamic scenes, we evaluated several alternative approaches and ultimately adopted VGGT, a feed-forward reconstruction method that proved more suitable for our experiments. Detailed comparative results of different trajectory estimation methods are provided in the supplementary material. *(2) Video Quality:* We evaluate video quality using the widely adopted VBench [18] metrics, reporting metrics across multiple dimensions, including Aesthetic Quality (Aes. Qual.), Imaging Quality (Img. Qual.), Temporal Flickering (Tem. Flick.), Motion Smoothness (Motion Smooth.), Subject Consistency (Sub. Cons.), and Background Consistency (Bg. Cons.). *(3) View Consistency:* We assess view consistency between generated and real videos in the feature space using Fréchet Image Distance (FID) [14] and Fréchet Video Distance (FVD) [33]. For real-world datasets, we measure the similarity between generated videos and their corresponding source videos. For synthetic datasets, we compare directly against ground-truth target videos.

Method	Camera Accuracy		Video Quality						View Consistency	
	Rot Err↓	Trans Err↓	Aes. Qual.↑	Img. Qual.↑	Tem. Flick.↑	Motion Smooth.↑	Sub. Cons.↑	Bg. Cons.↑	FID↓	FVD↓
DaS [10]	0.0724	0.4872	52.43	61.69	**96.98**	98.94	93.39	92.56	101.75	474.29
TrajectoryCrafter [25]	0.0851	0.2154	51.69	59.53	95.31	98.15	90.37	91.28	114.71	478.55
ReCamMaster [3]	0.0649	0.1480	52.23	62.61	96.15	98.89	92.97	91.89	85.68	421.97
PostCam	**0.0501**	**0.1021**	**53.52**	**65.71**	96.08	**99.01**	**94.03**	**92.58**	**67.20**	**380.96**

Table 1: Quantitative comparison with state-of-the-art methods on the OpenViD dataset.

Method	Camera Accuracy		Video Quality						View Consistency	
	Rot Err↓	Trans Err↓	Aes. Qual.↑	Img. Qual.↑	Tem. Flick.↑	Motion Smooth.↑	Sub. Cons.↑	Bg. Cons.↑	FID↓	FVD↓
DaS [10]	0.1112	0.9010	49.41	52.62	**96.25**	98.67	84.55	89.58	363.52	988.56
TrajectoryCrafter [25]	0.0924	0.2653	51.64	50.77	94.11	97.62	83.54	89.50	250.91	799.15
ReCamMaster [3]	0.0638	0.1437	58.50	63.31	95.98	99.08	91.13	91.65	103.74	434.34
PostCam	**0.0495**	**0.0791**	**59.80**	**64.64**	96.17	**99.13**	**92.48**	**93.15**	**80.29**	**313.02**

Table 2: Quantitative comparison with state-of-the-art methods on the synthetic dataset.

Table 3: User study results (mean ± standard deviation).

Method	Vis. Qual.	Control	Consist.
DaS	1.82±1.06	1.48±0.76	1.57±0.90
TrajCrafter	2.19 ±1.11	2.20 ±1.21	2.10 ± 1.17
ReCamMaster	3.38±0.93	3.52±0.89	3.31± 0.96
PostCam	**4.42±0.57**	**4.41±0.64**	**4.49±0.56**

4.2 Comparison with State-of-the-Art Methods

We compare PostCam with state-of-the-art camera-conditioned video generation methods: DaS [10], TrajectoryCrafter [25], and ReCamMaster [3]. To ensure a fair evaluation, a unified preprocessing pipeline is applied to all generated videos to standardize their spatial resolution and temporal length. Specifically, all baselines are first generated using their official configurations (e.g., ReCamMaster at 81 frames) and subsequently normalized to a uniform duration of 41 frames through frame sampling. For spatial consistency, we crop and resize all outputs to a 480×720 resolution, following the protocol of DaS due to its minimal aspect ratio. This ensures that the initial frames across all methods contain identical visual information, preventing extraneous content from biasing the comparison.

As shown in Table 1 and Table 2, PostCam substantially outperforms the baseline methods in camera-control accuracy while simultaneously achieving state-of-the-art performance on most video-quality metrics. Qualitative results in Fig. 5 further highlight these advantages. Additional qualitative comparisons, including examples on OpenViD, synthetic data, and in-the-wild scenes, can be found in the supplementary materials and supplementary video.

4.2.1 Robustness to Depth Noise. To evaluate the robustness to depth noise, we add Gaussian noise of varying strengths to the point cloud before rendering. As shown in Fig. 7, our method remains highly robust, whereas the performance of TrajectoryCrafter degrades significantly.

4.2.2 User Study. We conduct a blind user study based on Mean Opinion Score (MOS) with 20 participants, comparing PostCam against ReCamMaster, TrajectoryCrafter, and DaS. Participants rate the videos on a scale of 1–5 across three dimensions: visual quality, camera controllability, and temporal consistency. As shown in Table 3, PostCam outperforms all baselines across all dimensions, validating that the improvements in automated metrics are consistent with human perception.

4.3 Ablation Study

4.3.1 Ablation on Conditioning Strategies. To evaluate the impact of different conditioning strategies, we implement the following variants under identical training settings:

Pose-only: uses only camera parameters as the control signal, injected via cross-attention.

Render-only: uses only the rendered video, encoded with 3D self-attention and injected via cross-attention.

Baseline Fusion (RT+Render): employs both camera parameters and rendered video, where each modality is encoded independently and injected into the network through its own dedicated cross-attention layer in a single stage.

Baseline Fusion (Plücker+Render): uses Plücker coordinates and rendered video. Following several image-to-video methods [7, 8] that fuse camera poses and rendered frames, we implement a video-to-video version in which the Plücker information is added to the noised latents and the rendered video is injected through cross-attention in a single stage.

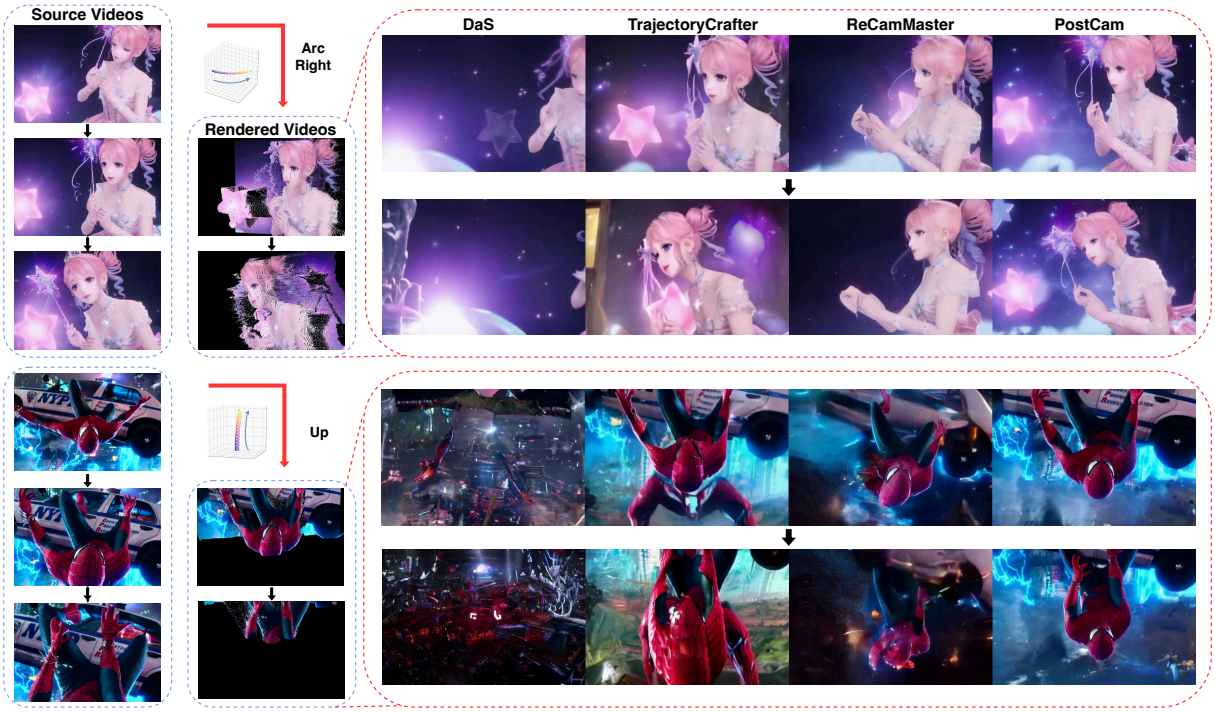


Figure 5: Qualitative comparison results. Column 1 displays source frames (initial, middle, final), while column 2 illustrates target camera motions (direction and rendering). Columns 3–6 compare our method against leading approaches. As an I2V model, DaS fails to maintain temporal coherence. TrajectoryCrafter is sensitive to rendering quality, showing artifacts when depth data is inaccurate or incomplete (e.g., the missing head in Scene 2). While ReCamMaster is render-agnostic, it fails to balance visual quality with motion precision in complex scenarios. In contrast, our method robustly generates high-quality results that faithfully align with source content and achieve superior pose accuracy.

Our main model is *PostCam (RT+Render)*. We additionally implement a variant, *PostCam (Plücker+Render)*, which uses Plücker coordinates as input. This variant also adopts the query-shared cross-attention module and the two-stage training strategy.

Table 4 demonstrates that a direct combination of both signals is suboptimal. Notably, the RT+Render baseline fails to converge effectively, resulting in the least accurate motion control among all tested configurations under equal training iterations. We attribute this to the significant disparity between pose trajectories and rendered video information. Simultaneously injecting these two heterogeneous signals makes it difficult for the model to converge. Converting camera poses into Plücker coordinates for injection partially alleviates the convergence issue—this also explains why most I2V methods adopt Plücker coordinates. However, this approach remains a suboptimal injection strategy.

In contrast, our method, which employs query-shared cross-attention, effectively extracts the essential and shared camera motion information from different modalities. This mechanism is agnostic to the pose representation, functioning robustly regardless of whether poses are expressed as camera parameters (RT) or Plücker coordinates. As shown in the table, our approach achieves state-of-the-art performance in both camera control accuracy and generation quality.

Method	Camera Accuracy		Video Quality	
	RotErr↓	TransErr↓	Aes. Qual.↑	Img. Qual.↑
Pose-only	0.0841	0.1545	58.15	63.63
Render-only	0.0548	0.1786	57.22	62.63
Baseline Fusion(Plücker+Render)	0.0727	0.2312	58.61	**64.95**
Baseline Fusion(RT+Render)	0.1140	0.3718	58.12	62.73
PostCam(Plücker+Render)	**0.0465**	0.1259	58.70	64.83
PostCam(RT+Render)	0.0495	**0.0791**	**59.80**	64.64

Table 4: Ablation study on the synthetic dataset evaluating different camera conditioning strategies.

Specifically, through a single shared query, the model selectively extracts the most beneficial components from both modalities: it first learns fundamental motion patterns solely from camera poses and then incorporates richer visual cues from rendered videos for fine-grained control and quality enhancement. This progressive learning strategy, combined with the shared query mechanism, effectively resolves the aforementioned convergence difficulties and modal conflicts. The qualitative results in Fig. 6 further corroborate our findings.

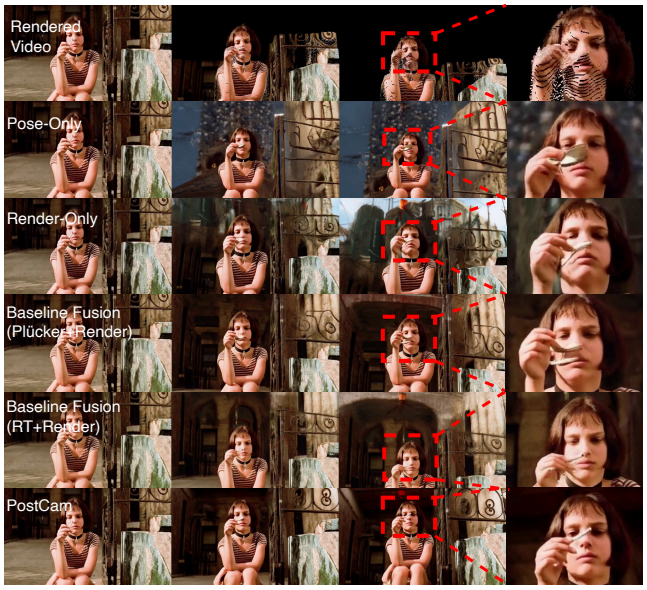


Figure 6: Comparisons under different conditions. Our method achieves faithful preservation of fine details and more accurate background generation while ensuring accurate camera motion control. The red boxes highlight that, even when distortions occur in the rendered views, only our results retain fine details, such as the cigarette in the hand, while achieving superior pose accuracy.

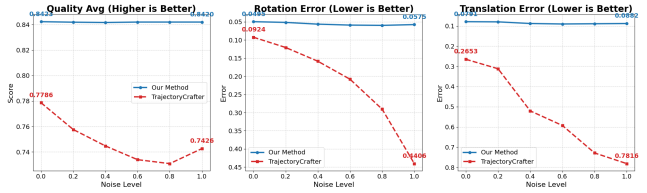


Figure 7: Comparison of VBench quality average (left), rotation error (middle), and translation error (right) under varying depth noise levels.

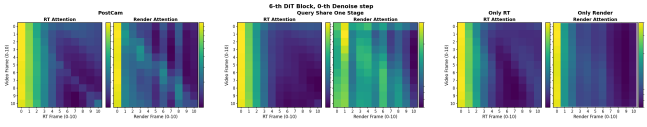


Figure 8: Attention Distribution Comparison.

4.3.2 Ablation on Query-Shared Cross-Attention. To quantify the contribution of the proposed query-shared cross-attention, we ablate three condition injection strategies while keeping the training settings (including the two-stage training strategy) and input data identical. *w/o query-shared*: each transformer block employs two separate cross-attention layers, one for camera parameters and another for the rendered condition. *w/o kv-concatenated*: the query matrix is shared, but the keys and values of the two conditions are processed independently and injected into the noise via the same query. *Ours*: the query matrix is shared and the key–value pairs of both conditions are concatenated before attention computation.

Method	Camera Accuracy		Video Quality	
	RotErr↓	TransErr↓	Aes. Qual.↑	Img. Qual.↑
w/o query-shared	0.1386	0.1707	59.13	**65.94**
w/o kv-concatenated	0.1389	0.1984	59.33	65.90
Ours	**0.0495**	**0.0791**	**59.80**	64.64

Table 5: Ablation study on the synthetic dataset evaluating different attention injection mechanisms.

Method	Camera Accuracy		Video Quality	
	RotErr↓	TransErr↓	Aes. Qual.↑	Img. Qual.↑
one stage	0.0578	0.1299	58.98	**65.05**
two stage, render-first	0.0991	0.1730	56.89	63.08
two stage, pose-first	**0.0495**	**0.0791**	**59.80**	64.64

Table 6: Ablation study on the synthetic dataset evaluating different training strategies.

For a fair comparison, all strategies undergo the same two-stage training pipeline. As reported in Table 5, the proposed query-shared cross-attention achieves the highest camera-motion control accuracy. Under the shared-query design, the module first computes an attention matrix from the query and the concatenated key features. A subsequent softmax operation produces a weighted distribution that assigns higher importance to features most relevant to the video generation task. These weights govern the selective aggregation of information from the concatenated value features, enabling the module to distill common camera motion cues for both precise pose control and high-fidelity generation. Qualitative results can be found in the supplementary material.

4.3.3 Ablation on Two-Stage Training. To validate the efficacy of the proposed two-stage training, we ablate three strategies: (1) *one stage*, which directly trains on both camera-control conditions; (2) *two stage, render-first*, which employs only the rendered condition in the first stage and both conditions in the second; and (3) *two stage, pose-first* (i.e., ours), which employs only the pose condition in the first stage and both conditions in the second. As shown in Table 6, our two-stage training achieves the best camera control among the three variants. In the one-stage case, the model must simultaneously learn from multiple control conditions, leading to suboptimal camera-control accuracy. In the render-first two-stage case, the model tends to enforce pixel-level alignment between the rendered frames and the synthesized output rather than learning the underlying camera motion, resulting in degraded pose controllability. By contrast, our approach enables the model to first learn the underlying camera motion from poses alone and subsequently incorporate rendered videos for finer motion control and enhanced visual fidelity.

4.3.4 Attention Distribution Comparison. The attention maps in Fig. 8 validate the contributions of our full PostCam model. PostCam (left) exhibits the clearest diagonal structure, signifying precise and temporally consistent cross-frame attention. This structured pattern progressively breaks down as key components are removed. Eliminating the two-stage training (Query Share One Stage, middle) noticeably degrades the diagonal. Furthermore, when both

two-stage training and query sharing are removed (Only RT and Only Render, right), the diagonal structure is nearly eradicated, resulting in highly diffuse attention maps. This lack of focused temporal structure directly visualizes how these ablated models are significantly more prone to overfitting to irrelevant signals.

5 Conclusion

We propose PostCam, a novel-view video generation framework for dynamic scenes that enables precise post-capture editing of camera trajectories. To address the limitations of existing methods, including low camera control accuracy and inadequate detail preservation, we introduce a query-shared cross-attention module combined with a two-stage training strategy, which significantly enhances the understanding and manipulation of camera motion. Experiments on both real-world and synthetic datasets demonstrate that PostCam surpasses current state-of-the-art methods, achieving over 20% improvement in camera control precision and view consistency while delivering the highest video generation quality.

References

[1] Sherwin Bahmani, Ivan Skorokhodov, Guocheng Qian, Aliaksandr Siarohin, Willi Menapace, Andrea Tagliasacchi, David B Lindell, and Sergey Tulyakov. 2025. Ac3d: Analyzing and improving 3d camera control in video diffusion transformers. In *Proceedings of the Computer Vision and Pattern Recognition Conference*. 22875–22889.

[2] Sherwin Bahmani, Ivan Skorokhodov, Aliaksandr Siarohin, Willi Menapace, Guocheng Qian, Michael Vasilkovsky, Hsin-Ying Lee, Chaoyang Wang, Jiaxu Zou, Andrea Tagliasacchi, et al. 2024. Vd3d: Taming large video diffusion transformers for 3d camera control. *arXiv preprint arXiv:2407.12781* (2024).

[3] Jianhong Bai, Menghan Xia, Xiao Fu, Xintao Wang, Lianrui Mu, Jinwen Cao, Zuozhu Liu, Haoji Hu, Xiang Bai, Pengfei Wan, et al. 2025. Recammaster: Camera-controlled generative rendering from a single video. *arXiv preprint arXiv:2503.11647* (2025).

[4] Weikang Bian, Zhaoyang Huang, Xiaoyu Shi, Yijin Li, Fu-Yun Wang, and Hongsheng Li. 2025. GS-DiT: Advancing Video Generation with Pseudo 4D Gaussian Fields through Efficient Dense 3D Point Tracking. *arXiv preprint arXiv:2501.02690* (2025).

[5] Andreas Blattmann, Tim Dockhorn, Sumith Kulal, Daniel Mendelevitch, Maciej Kilian, Dominik Lorenz, Yam Levi, Zion English, Vikram Voleti, Adam Letts, et al. 2023. Stable video diffusion: Scaling latent video diffusion models to large datasets. *arXiv preprint arXiv:2311.15127* (2023).

[6] Tim Brooks, Bill Peebles, Connor Holmes, Will DePue, Yufei Guo, Li Jing, David Schnurr, Joe Taylor, Troy Luhman, Eric Luhman, et al. 2024. Video generation models as world simulators. *OpenAI Blog* 1 (2024), 8.

[7] Chenjie Cao, Chaohui Yu, Shang Liu, Fan Wang, Xiangyang Xue, and Yanwei Fu. 2025. MVGenMaster: Scaling Multi-View Generation from Any Image via 3D Priors Enhanced Diffusion Model. In *Proceedings of the Computer Vision and Pattern Recognition Conference*. 6045–6056.

[8] Chenjie Cao, Jingkai Zhou, Shikai Li, Jingyun Liang, Chaohui Yu, Fan Wang, Xiangyang Xue, and Yanwei Fu. 2025. Uni3C: Unifying Precisely 3D-Enhanced Camera and Human Motion Controls for Video Generation. *arXiv preprint arXiv:2504.14899* (2025).

[9] Wanquan Feng, Jiawei Liu, Pengqi Tu, Tianhao Qi, Mingzhen Sun, Tianxiang Ma, Songtao Zhao, Siyu Zhou, and Qian He. 2024. I2VControl-Camera: Precise Video Camera Control with Adjustable Motion Strength. *arXiv preprint arXiv:2411.06525* (2024).

[10] Zekai Gu, Rui Yan, Jiahao Lu, Peng Li, Zhiyang Dou, Chenyang Si, Zhen Dong, Qifeng Liu, Cheng Lin, Ziwei Liu, et al. 2025. Diffusion as Shader: 3D-aware Video Diffusion for Versatile Video Generation Control. *arXiv preprint arXiv:2501.03847* (2025).

[11] Yuwei Guo, Ceyuan Yang, Anyi Rao, Zhengyang Liang, Yaohui Wang, Yu Qiao, Maneesh Agrawala, Dahua Lin, and Bo Dai. 2023. Animatediff: Animate your personalized text-to-image diffusion models without specific tuning. *arXiv preprint arXiv:2307.04725* (2023).

[12] Hao He, Yinghao Xu, Yuwei Guo, Gordon Wetzstein, Bo Dai, Hongsheng Li, and Ceyuan Yang. 2024. Cameractrl: Enabling camera control for text-to-video generation. *arXiv preprint arXiv:2404.02101* (2024).

[13] Hao He, Ceyuan Yang, Shanchuan Lin, Yinghao Xu, Meng Wei, Liangke Gui, Qi Zhao, Gordon Wetzstein, Lu Jiang, and Hongsheng Li. 2025. Cameractrl ii: Dynamic scene exploration via camera-controlled video diffusion models. *arXiv preprint arXiv:2503.10592* (2025).

[14] Martin Heusel, Hubert Ramsauer, Thomas Unterthiner, Bernhard Nessler, and Sepp Hochreiter. 2017. Gans trained by a two time-scale update rule converge to a local nash equilibrium. *Advances in neural information processing systems* 30 (2017).

[15] Jonathan Ho, Tim Salimans, Alexey Gritsenko, William Chan, Mohammad Norouzi, and David J Fleet. 2022. Video diffusion models. *Advances in Neural Information Processing Systems* 35 (2022), 8633–8646.

[16] Chen Hou, Guoqiang Wei, Yan Zeng, and Zhibo Chen. 2024. Training-free camera control for video generation. *arXiv preprint arXiv:2406.10126* (2024).

[17] Teng Hu, Jiangning Zhang, Ran Yi, Yating Wang, Hongrui Huang, Jieyu Weng, Yabiao Wang, and Lizhuang Ma. 2024. Motionmaster: Training-free camera motion transfer for video generation. *arXiv preprint arXiv:2404.15789* (2024).

[18] Ziqi Huang, Yinan He, Jiashuo Yu, Fan Zhang, Chenyang Si, Yuming Jiang, Yuanhan Zhang, Tianxing Wu, Qingyang Jin, Nattapol Chanpaisit, et al. 2024. Vbench: Comprehensive benchmark suite for video generative models. In *Proceedings of the IEEE/CVF Conference on Computer Vision and Pattern Recognition*. 21807–21818.

[19] Weijie Kong, Qi Tian, Zijian Zhang, Rox Min, Zuozhuo Dai, Jin Zhou, Jiangfeng Xiong, Xin Li, Bo Wu, Jianwei Zhang, et al. 2024. Hunyuanvideo: A systematic framework for large video generative models. *arXiv preprint arXiv:2412.03603* (2024).

[20] Zhengfei Kuang, Shengqu Cai, Hao He, Yinghao Xu, Hongsheng Li, Leonidas J Guibas, and Gordon Wetzstein. 2024. Collaborative video diffusion: Consistent multi-video generation with camera control. *Advances in Neural Information Processing Systems* 37 (2024), 16240–16271.

[21] Teng Li, Guangcong Zheng, Rui Jiang, Tao Wu, Yehao Lu, Yining Lin, Xi Li, et al. 2025. Realcam-i2v: Real-world image-to-video generation with interactive complex camera control. *arXiv preprint arXiv:2502.10059* (2025).

[22] Hanwen Liang, Junli Cao, Vidit Goel, Guocheng Qian, Sergei Korolev, Demetri Terzopoulos, Konstantinos N Plataniotis, Sergey Tulyakov, and Jian Ren. 2025. Wonderland: Navigating 3d scenes from a single image. In *Proceedings of the Computer Vision and Pattern Recognition Conference*. 798–810.

[23] Pengyang Ling, Jiazi Bu, Pan Zhang, Xiaoyi Dong, Yuhang Zang, Tong Wu, Huaian Chen, Jiaqi Wang, and Yi Jin. 2024. Motionclone: Training-free motion cloning for controllable video generation. *arXiv preprint arXiv:2406.05338* (2024).

[24] Yaron Lipman, Ricky TQ Chen, Heli Ben-Hamu, Maximilian Nickel, and Matt Le. 2022. Flow matching for generative modeling. *arXiv preprint arXiv:2210.02747* (2022).

[25] YU Mark, Wenbo Hu, Jinbo Xing, and Ying Shan. 2025. Trajectorycrafter: Redirecting camera trajectory for monocular videos via diffusion models. *arXiv preprint arXiv:2503.05638* 2 (2025).

[26] Norman Müller, Katja Schwarz, Barbara Rössle, Lorenzo Porzi, Samuel Rota Bulò, Matthias Nießner, and Peter Kontschieder. 2024. Multidiff: Consistent novel view synthesis from a single image. In *Proceedings of the IEEE/CVF Conference on Computer Vision and Pattern Recognition*. 10258–10268.

[27] Kepan Nan, Rui Xie, Penghao Zhou, Tiehan Fan, Zhenheng Yang, Zhijie Chen, Xiang Li, Jian Yang, and Ying Tai. 2024. Openvid-1m: A large-scale high-quality dataset for text-to-video generation. *arXiv preprint arXiv:2407.02371* (2024).

[28] William Peebles and Saining Xie. 2023. Scalable diffusion models with transformers. In *Proceedings of the IEEE/CVF international conference on computer vision*. 4195–4205.

[29] Stefan Popov, Amit Raj, Michael Krainin, Yuanzhen Li, William T Freeman, and Michael Rubinstein. 2025. CamCtrl3D: Single-Image Scene Exploration with Precise 3D Camera Control. *arXiv preprint arXiv:2501.06006* (2025).

[30] Xuanchi Ren, Tianchang Shen, Jiahui Huang, Huan Ling, Yifan Lu, Merlin Nimier-David, Thomas Müller, Alexander Keller, Sanja Fidler, and Jun Gao. 2025. Gen3c: 3d-informed world-consistent video generation with precise camera control. In *Proceedings of the Computer Vision and Pattern Recognition Conference*. 6121–6132.

[31] Johannes Lutz Schönberger and Jan-Michael Frahm. 2016. Structure-from-Motion Revisited. In *Conference on Computer Vision and Pattern Recognition (CVPR)*.

[32] Uriel Singer, Adam Polyak, Thomas Hayes, Xi Yin, Jie An, Songyang Zhang, Qiyuan Hu, Harry Yang, Oron Ashual, Oran Gafni, et al. 2022. Make-a-video: Text-to-video generation without text-video data. *arXiv preprint arXiv:2209.14792* (2022).

[33] Thomas Unterthiner, Sjoerd van Steenkiste, Karol Kurach, Raphael Marinier, Marcin Michalski, and Sylvain Gelly. 2018. FVD: A New Metric for Video Generation. *arXiv preprint arXiv:1812.01717* (2018).

[34] Basile Van Hoorick, Rundi Wu, Ege Ozguroglu, Kyle Sargent, Ruoshi Liu, Pavel Tokmakov, Achal Dave, Changxi Zheng, and Carl Vondrick. 2024. Generative camera dolly: Extreme monocular dynamic novel view synthesis. In *European Conference on Computer Vision*. Springer, 313–331.

[35] Team Wan, Ang Wang, Baole Ai, Bin Wen, Chaojie Mao, Chen-Wei Xie, Di Chen, Feiwu Yu, Haiming Zhao, Jianxiao Yang, et al. 2025. Wan: Open and advanced large-scale video generative models. *arXiv preprint arXiv:2503.20314* (2025).

[36] Jianyuan Wang, Minghao Chen, Nikita Karaev, Andrea Vedaldi, Christian Rupprecht, and David Novotny. 2025. Vggt: Visual geometry grounded transformer. In *Proceedings of the Computer Vision and Pattern Recognition Conference*. 5294–5306.

[37] Yuelei Wang, Jian Zhang, Pengtao Jiang, Hao Zhang, Jinwei Chen, and Bo Li. 2024. CPA: Camera-pose-awareness diffusion transformer for video generation. *arXiv preprint arXiv:2412.01429* (2024).

[38] Yifan Wang, Jianjun Zhou, Haoyi Zhu, Wenzheng Chang, Yang Zhou, Zizun Li, Junyi Chen, Jiangmiao Pang, Chunhua Shen, and Tong He. 2025. π^3: Scalable Permutation-Equivariant Visual Geometry Learning. arXiv:2507.13347 [cs.CV] https://arxiv.org/abs/2507.13347

[39] Zhouxia Wang, Ziyang Yuan, Xintao Wang, Yaowei Li, Tianshui Chen, Menghan Xia, Ping Luo, and Ying Shan. 2024. Motionctrl: A unified and flexible motion controller for video generation. In *ACM SIGGRAPH 2024 Conference Papers*. 1–11.

[40] Zeqi Xiao, Wenqi Ouyang, Yifan Zhou, Shuai Yang, Lei Yang, Jianlou Si, and Xingang Pan. 2024. Trajectory Attention for Fine-grained Video Motion Control. *arXiv preprint arXiv:2411.19324* (2024).

[41] Zeqi Xiao, Yifan Zhou, Shuai Yang, and Xingang Pan. 2024. Video diffusion models are training-free motion interpreter and controller. *arXiv preprint arXiv:2405.14864* (2024).

[42] Dejia Xu, Weili Nie, Chao Liu, Sifei Liu, Jan Kautz, Zhangyang Wang, and Arash Vahdat. 2024. Camco: Camera-controllable 3d-consistent image-to-video generation. *arXiv preprint arXiv:2406.02509* (2024).

[43] Zhuoyi Yang, Jiayan Teng, Wendi Zheng, Ming Ding, Shiyu Huang, Jiazheng Xu, Yuanming Yang, Wenyi Hong, Xiaohan Zhang, Guanyu Feng, et al. 2024. Cogvideox: Text-to-video diffusion models with an expert transformer. *arXiv preprint arXiv:2408.06072* (2024).

[44] Hidir Yesiltepe and Pinar Yanardag. 2025. Dynamic View Synthesis as an Inverse Problem. *arXiv preprint arXiv:2506.08004* (2025).

[45] Wangbo Yu, Jinbo Xing, Li Yuan, Wenbo Hu, Xiaoyu Li, Zhipeng Huang, Xiangjun Gao, Tien-Tsin Wong, Ying Shan, and Yonghong Tian. 2024. Viewcrafter: Taming video diffusion models for high-fidelity novel view synthesis. *arXiv preprint arXiv:2409.02048* (2024).

[46] Shangjin Zhai, Zhichao Ye, Jialin Liu, Weijian Xie, Jiaqi Hu, Zhen Peng, Hua Xue, Danpeng Chen, Xiaomeng Wang, Lei Yang, et al. 2025. StarGen: A Spatiotemporal Autoregression Framework with Video Diffusion Model for Scalable and Controllable Scene Generation. *arXiv preprint arXiv:2501.05763* (2025).

[47] David Junhao Zhang, Roni Paiss, Shiran Zada, Nikhil Karnad, David E Jacobs, Yael Pritch, Inbar Mosseri, Mike Zheng Shou, Neal Wadhwa, and Nataniel Ruiz. 2025. Recapture: Generative video camera controls for user-provided videos using masked video fine-tuning. In *Proceedings of the Computer Vision and Pattern Recognition Conference*. 2050–2062.

[48] Guangcong Zheng, Teng Li, Rui Jiang, Yehao Lu, Tao Wu, and Xi Li. 2024. Cami2v: Camera-controlled image-to-video diffusion model. *arXiv preprint arXiv:2410.15957* (2024).

[49] Zangwei Zheng, Xiangyu Peng, Tianji Yang, Chenhui Shen, Shenggui Li, Hongxin Liu, Yukun Zhou, Tianyi Li, and Yang You. 2024. Open-sora: Democratizing efficient video production for all. *arXiv preprint arXiv:2412.20404* (2024).

A Synthetic Dataset

Synchronized multi-view videos of dynamic scenes are difficult to capture in the real world. To address this, we created a lightweight synthetic benchmark where each test sample (source video + target trajectory) pairs with a ground-truth target video rendered from the same scene and animation, differing only by camera viewpoint. This design enables systematic evaluation of PostCam's camera-control accuracy. As can be seen in Fig. 9, all characters and scenes originate from the official asset library of Unreal Engine 5, ultimately composing ten dynamic scenes featuring distinct styles and characters. For each scene, we randomly sampled ten start–end camera poses within the navigable space and smoothly interpolated them with quadratic Bézier curves to produce 100-frame 1920×1080 trajectories; small Gaussian noise added to the control points further diversifies the motions. Beyond RGB frames, we also rendered depth and normal maps for each frame. These were not used in our evaluation (where VGGT-estimated depth was used), but are provided for future research. The dataset and complete generation scripts will be publicly released. Qualitative comparisons on the synthetic dataset are also presented in Fig. 10, where each row shows the source video, the ground-truth target view, and results from different methods. The results visually highlight PostCam's advantages in camera pose accuracy and cross-view consistency.

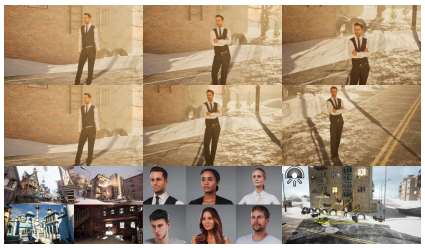


Figure 9: Synthetic test dataset. The first two rows depict a dynamic scene from the synthetic test dataset under different camera trajectories. The final row presents representative examples of the scene layout, character appearance, and the intermediate rendering process.

B Evaluation of Camera Pose Estimation Methods

In this section, we provide a detailed evaluation of various camera pose estimation methods to justify the selection of VGGT [36] for our pipeline.

We conducted our evaluation on our synthetic test set. The protocol involved processing the videos with each pose estimation method to compute the camera trajectory. The predicted trajectory was then compared against the ground-truth camera trajectory provided by the dataset. We use standard metrics for evaluation: Rotational Error(denotes Rot. Err.) and Translational Error(denotes Trans. Err.).

We evaluated conventional Structure-from-Motion methods, including COLMAP [31], dynamic-scene-oriented models Pi3 [38], and VGGT [36].

We observed that conventional Structure-from-Motion methods, struggle significantly with the dynamic elements present in our test videos. These methods frequently failed to reconstruct the camera poses correctly, exhibiting a low success rate of approximately 30%.

In contrast, both VGGT and Pi3 performed more robustly. As shown in Table 7, reveals that VGGT is more suitable for our experiments. Based on this evidence, we selected VGGT as the core pose estimation method for all experiments presented in the main paper.

Table 7: Comparison of Pose Estimation Accuracy on Synthetic Dynamic Scenes

Method	Rot. Err.	Trans. Err.	Notes
COLMAP	-	-	Low success rate (~30%)
Pi3	0.0304	0.0352	-
VGGT (Ours)	**0.0275**	**0.0241**	-

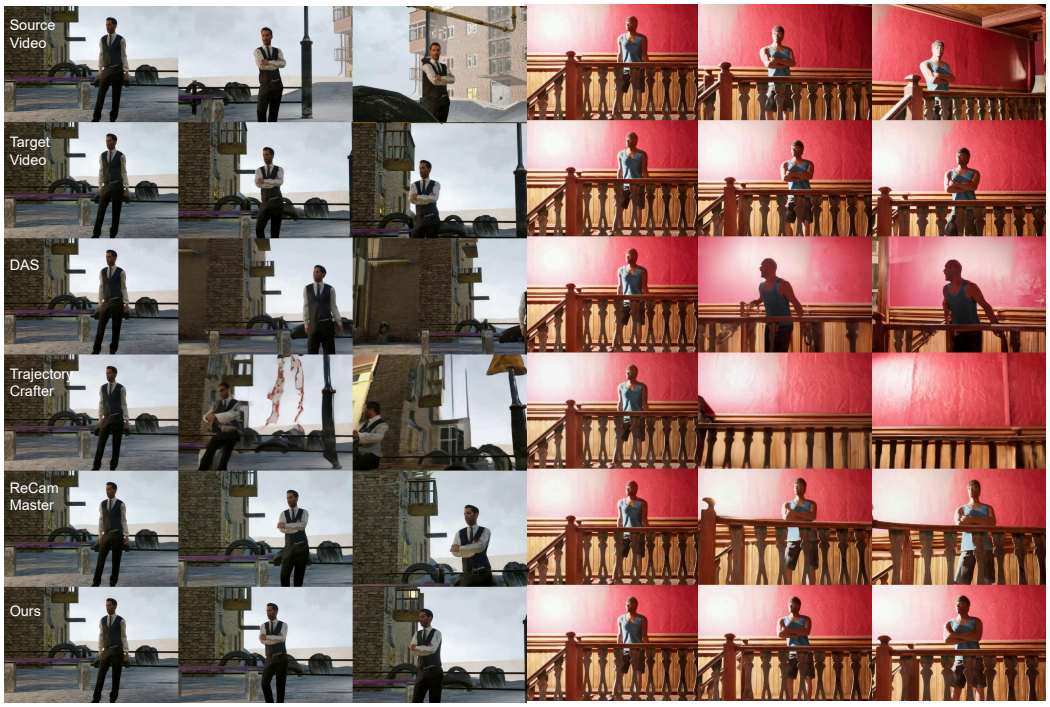


Figure 10: Qualitative comparison results in synthetic dataset. Each row corresponds to a different method; the first two rows show the source video and the ground-truth target view, respectively. PostCam produces noticeably higher-quality results than other methods, and its alignment with the target view further highlights its superior camera control accuracy.



Figure 11: Qualitative comparison results in OpenVid dataset. Two test sequences from the OpenVid dataset. Each row represents a different method, with the last row showing the original input video. In the first sequence, only our method preserves consistent facial features across frames, while other methods show identity shifts or visual artifacts. In the second sequence, only our method maintains detailed hand structures, avoiding the warping seen in baseline results. Red dashed boxes indicate regions that highlight the strengths of our approach.



Figure 12: Comparisons under different attention mechanism. Each row corresponds to a different method; the first two rows show the source videos and the rendered videos. By examining the motion consistency with the rendered videos, it is evident that all ablated variants perform significantly worse than PostCam, showing the effectiveness of the proposed query-shared cross-attention in enhancing pose accuracy. The higher image quality scores observed on VBench are primarily a consequence of poor camera control, which leads to reduced camera motion. With less camera movement, the generated video becomes more static, enabling a larger portion of the scene to be directly reused from the source video. This simplifies the generation task and artificially inflates the image quality metrics.